



TITLE:

# Accuracy verification of infrared marker-based dynamic tumor-tracking irradiation using the gimbaled x-ray head of the Vero4DRT (MHI-TM2000).

AUTHOR(S):

Mukumoto, Nobutaka; Nakamura, Mitsuhiro; Sawada, Akira; Suzuki, Yasunobu; Takahashi, Kunio; Miyabe, Yuki; Kaneko, Shuji; Mizowaki, Takashi; Kokubo, Masaki; Hiraoka, Masahiro

---

CITATION:

Mukumoto, Nobutaka ...[et al]. Accuracy verification of infrared marker-based dynamic tumor-tracking irradiation using the gimbaled x-ray head of the Vero4DRT (MHI-TM2000).. Medical physics 2013, 40(4): 41706.

ISSUE DATE:

2013-04

URL:

<http://hdl.handle.net/2433/189832>

RIGHT:

© 2013 American Association of Physicists in Medicine; この論文は出版社版ではありません。引用の際には出版社版をご確認ご利用ください。;  
This is not the published version. Please cite only the published version.

## Accuracy verification of IR Tracking with the Vero4DRT

**Accuracy verification of infrared marker-based dynamic tumor-tracking irradiation using the gimbaled x-ray head of the Vero4DRT (MHI-TM2000)**

5 Nobutaka Mukumoto<sup>1</sup>, Mitsuhiro Nakamura<sup>\*1</sup>, Akira Sawada<sup>1,2</sup>, Yasunobu Suzuki<sup>3</sup>,  
Kunio Takahashi<sup>1,3</sup>, Yuki Miyabe<sup>1</sup>, Shuji Kaneko<sup>1,3</sup>, Takashi Mizowaki<sup>1</sup>, Masaki  
Kokubo<sup>4,5</sup>, and Masahiro Hiraoka<sup>1</sup>

<sup>1</sup>Department of Radiation Oncology and Image-applied Therapy, Graduate School of  
10 Medicine, Kyoto University, Kyoto 606-8507, Japan

<sup>2</sup>Department of Radiological Technology, Faculty of Medical Science, Kyoto College of  
Medical Science, Nantan 622-0041, Japan

<sup>3</sup>Advanced Mechanical Systems Department, Mitsubishi Heavy Industries Ltd., Hiroshima  
733-8553, Japan

15 <sup>4</sup>Department of Radiation Oncology, Kobe City Medical Center General Hospital, Kobe  
650-0047, Japan

<sup>5</sup>Division of Radiation Oncology, Institute of Biomedical Research and Innovation, Kobe  
650-0047, Japan

20 **\*Corresponding author:** Mitsuhiro Nakamura, Ph.D., Graduate School of Medicine, Kyoto  
University, 54 Kawahara-cho, Shogoin, Sakyo-ku, Kyoto, 606-8507, Japan.

Tel.: +81-75-751-3762; Fax: +81-75-771-9749; E-mail: m\_nkmr@kuhp.kyoto-u.ac.jp

**Running title:** Accuracy verification of IR Tracking with the Vero4DRT.

## Accuracy verification of IR Tracking with the Vero4DRT

**Conflicts of interest:** This research was in part sponsored by Mitsubishi Heavy Industries, Ltd., Japan. Takashi Mizowaki, Masaki Kokubo, and Masahiro Hiraoka have consultancy agreements with Mitsubishi Heavy Industries, Ltd., Japan.

- 30 **Meeting presentation:** This research was presented orally, in part, at the American Association of Physicists in Medicine (AAPM) 54<sup>th</sup> Annual Meeting in Charlotte, July 29 to August 2, 2012.

## Accuracy verification of IR Tracking with the Vero4DRT

**Abstract**

**Purpose:** To verify the accuracy of an infrared (IR) marker-based dynamic tumor-tracking  
35 irradiation system (IR Tracking) using the gimbaled x-ray head of the Vero4DRT  
(MHI-TM2000).

**Methods and Materials:** The gimbaled 6-MV C-band x-ray head of the Vero4DRT can  
swing along the pan-and-tilt direction to track a moving target. During beam delivery, the  
Vero4DRT predicts the future three-dimensional (3D) target position in real time using a  
40 correlation model (4D model) between the target and IR marker motion, and then  
continuously transfers the corresponding tracking orientation to the gimbaled x-ray head. The  
4D-modeling error ( $E_{4DM}$ ) and the positional tracking error ( $E_P$ ) were defined as the  
difference between the predicted and measured positions of the target in 4D modeling and as  
the difference between the tracked and measured positions of the target during irradiation,  
45 respectively. For the clinical application of IR Tracking, we assessed the relationship between  
 $E_{4DM}$  and  $E_P$  for three 1D sinusoidal (peak-to-peak amplitude [ $A$ ]: 20-40 mm, breathing  
period [ $T$ ]: 2-4 s), five 1D phase-shifted sinusoidal ( $A$ : 20 mm,  $T$ : 4 s, phase shift [ $\tau$ ]: 0.2-2 s),  
and six 3D patient respiratory patterns.

**Results:** The difference between the 95<sup>th</sup> percentile of the absolute  $E_P$  ( $E_P^{95}$ ) and the mean ( $\mu$ )  
50 + two standard deviations (SD) of absolute  $E_{4DM}$  ( $E_{4DM}^{\mu+2SD}$ ) was within  $\pm 1$  mm for all motion  
patterns. As the absolute correlation between the target and IR marker motions decreased from  
1.0 to 0.1 for the 1D phase-shifted sinusoidal patterns, the  $E_{4DM}^{\mu+2SD}$  and  $E_P^{95}$  increased linearly,  
from 0.4 to 3.0 mm ( $R = -0.98$ ) and from 0.5 to 2.2 mm ( $R = -0.95$ ), respectively. There was a  
strong positive correlation between  $E_{4DM}^{\mu+2SD}$  and  $E_P^{95}$  in each direction [(lateral, craniocaudal,  
55 anteroposterior) = (0.99, 0.98, 1.00)], even for the 3D respiratory patterns; thus,  $E_P^{95}$  was  
readily estimated from  $E_{4DM}^{\mu+2SD}$ .

**Conclusions:** Positional tracking errors correlated strongly with 4D-modeling errors in IR



## Accuracy verification of IR Tracking with the Vero4DRT

Tracking. Thus, the accuracy of the 4D model must be verified before treatment, and margins are required to compensate for the 4D-modeling error.

60

Key words: Four-dimensional image-guided radiotherapy, dynamic tumor-tracking irradiation, intrafractional respiratory motion, gimbaled x-ray head, tracking accuracy.

## Accuracy verification of IR Tracking with the Vero4DRT

### I. INTRODUCTION

65           The International Commission on Radiation Units and Measurements (ICRU)  
recommends that the planning target volume (PTV) includes margins around a clinical target  
volume (CTV) to account for patient motion, tumor motion, and deformation due to  
respiration and uncertainties in beam placement.<sup>1,2</sup> Particularly for thoracic and abdominal  
tumors, respiration is an important factor causing uncertainty during beam delivery. Several  
70 techniques, including respiratory gating, breath-holding, and dynamic tumor tracking (DTT),  
have been proposed to reduce the uncertainties caused by respiratory motion.<sup>3</sup> Among these  
techniques, DTT can minimize the internal uncertainties without a prolonged treatment time  
or the burden of breath-holding for patients. There are two approaches to DTT: direct and  
indirect methods.<sup>3,4</sup> While direct methods detect the target itself, indirect methods assess  
75 some surrogate quantity and deduce localization information based on the surrogate.

We have developed a novel four-dimensional (4D) image-guided radiotherapy system  
with a DTT function: the Vero4DRT (MHI-TM2000; Mitsubishi Heavy Industries, Ltd., Japan,  
and BrainLAB, Feldkirchen, Germany).<sup>5-11</sup> Figure 1 shows a schematic diagram of the  
Vero4DRT. The Vero4DRT has several unique components that facilitate DTT irradiation: (1)  
80 a compact C-band 6-MV x-ray head with a gimbal mechanism, mounted on an O-ring gantry.  
The gimballed x-ray head can rotate in both the pan (horizontal to the O-ring) and tilt (vertical  
to the O-ring) directions, (2) a gantry-mounted orthogonal kV x-ray imaging subsystem,  
consisting of two sets of x-ray tubes and flat-panel detectors, with a spatial resolution of 0.2  
mm at the isocenter level, and (3) an extended version of the ExacTRAC system for the DTT  
85 function (BrainLAB)<sup>12,13</sup> with an infrared (IR) camera mounted on the ceiling of the treatment  
room.

The Vero4DRT is capable of direct and indirect DTT approaches. One is an x-ray  
image-based direct DTT approach (X-ray Tracking).<sup>9,10</sup> A moving tumor is tracked in real time

## Accuracy verification of IR Tracking with the Vero4DRT

by either direct monitoring of the tumor itself or fiducial markers, using the kV x-ray imaging  
90 subsystem. However, the x-ray monitoring interval and image processing time delay cause  
prediction errors.<sup>10</sup> Furthermore, continuous x-ray monitoring may result in two potential  
health hazards: deterministic and stochastic risks associated with the increased radiation dose  
delivered by the kV x-ray imaging subsystem.<sup>14-17</sup> The other is an IR marker-based indirect  
DTT approach (IR Tracking), which is available clinically. An advantage of IR Tracking is a  
95 substantial reduction in imaging dose, compared with that of X-ray Tracking. During beam  
delivery, the Vero4DRT monitors the displacement of the IR markers on the abdominal wall  
continuously via the IR camera of the ExacTRAC system, and then tracks target motion using a  
correlation model (4D model) between the target and IR marker motions, as described in  
Section II. A.

100 A key issue in indirect DTT is the accuracy of the model predicting the internal target  
position based on the surrogate measurements.<sup>3,4</sup> Several investigators have shown that the  
Synchrony Respiratory Tracking System, part of the Cyberknife indirect DTT system  
(Accuracy Inc., Sunnyvale, CA), was able to follow a moving tumor with high accuracy.<sup>18-22</sup>  
Depuydt *et al.* verified the positional tracking accuracy of IR Tracking only under conditions of  
105 a perfect correlation between the target and IR marker motions using a prototype of the  
Vero4DRT;<sup>13</sup> however, no dosimetric verification was performed. According to the report of  
the American Association of Physicists in Medicine Task Group 76, phase shifts between the  
internal tumor and external surrogate motion of  $> 1$  s were observed in patients with lung  
cancer.<sup>3</sup> The accuracy of a 4D model is unknown in the presence of such a phase shift.  
110 Additionally, tracking accuracy – based on the respiratory tumor and abdominal wall motions  
of real patients – should be verified before the clinical use of IR Tracking. Thus, in the present  
study, we verified the dosimetric and positional accuracy of IR Tracking.

## Accuracy verification of IR Tracking with the Vero4DRT

## 115 II. MATERIALS AND METHODS

### II. A. The 4D model for IR Tracking with the Vero4DRT

Figure 2 shows a schematic diagram of IR Tracking. Before irradiation, IR marker displacements on the abdominal wall and the implanted fiducial markers' motion are monitored to create a 4D model for 20-40 s using the IR camera of the ExacTRAC system every 16.7 ms and the orthogonal kV x-ray imaging subsystem every 80 ms, using a stereovision technique. After monitoring, two target positions are determined: the detected target position and the predicted target position. The detected target position is indicated by the centroid of the polyhedron, composed from the implanted fiducial markers. The predicted target position is calculated from the 4D model, expressed by a quadratic equation involving two variables, the position and velocity of the IR markers. In the 4D-modeling phase, the peak-to-peak amplitude of the detected target motion ( $A$ ) and the mean ( $\mu$ ) and standard deviation (SD) of the absolute difference between the detected and predicted target positions are automatically calculated along each axis (Fig. 2). During beam delivery, the 3D target position is calculated from the displacements of the IR markers using the 4D model, and then the corresponding tracking orientation is transferred continuously to the gimbaled x-ray head. The predicted target position can also be monitored visually in real time at a minimum interval of 1 s on intra-fractional fluoroscopic images.

### II. B. Dosimetric and positional verification of IR Tracking

For the clinical application of IR Tracking, the following verifications were performed:

- (1) Dosimetric and positional verification of 1D sinusoidal patterns with perfect correlation between the target and IR marker motions, using a motor-driven base.

## Accuracy verification of IR Tracking with the Vero4DRT

(2) Positional verification of 1D sinusoidal patterns with miscorrelation between the target and IR marker motions, using a dynamic anthropomorphic thorax phantom.

(3) Positional verification of 3D target and 1D surrogate motions, based on the patient's respiration, using a four-axis moving phantom.

### II. B. 1. Dosimetric and positional verification of IR Tracking for 1D sinusoidal patterns

Figure 3(a) shows a photograph of the experimental system for the dosimetric and positional verification of IR Tracking. The IR markers were moved synchronously with the 1D motor-driven base (QUASAR, Modus Medical Devices Inc., London, ON, Canada) in the anteroposterior (AP) direction.

Dosimetric verification was performed using EDR2 film (Kodak, Rochester, NY, USA), placed at a depth of 100 mm (1000 mm source-to-isocenter distance) in water-equivalent phantoms on the motor-driven base. Four pinholes were made on the film to identify the isocenter. The EDR2 film (Kodak, Rochester, NY, USA) was irradiated with a field size of  $50 \times 50 \text{ mm}^2$  under stationary, tracking, and non-tracking states for 1D sinusoidal patterns ( $A$ : 20-40 mm, breathing period  $[T]$ : 2-4 s) in the craniocaudal (CC) direction. In total, seven irradiated films were scanned in the same orientation (ES-10000G; Epson Corp., Nagano, Japan) with a resolution of 150 dpi in 16-bit grayscale with a 12-h postexposure period. All films were analyzed using commercially available radiation dosimetry software (DD system, ver. 9.4; R'Tech Inc., Tokyo, Japan). Differences in the width of the 95% dose profile between stationary and moving conditions ( $E_D^{95}$ ) were calculated.

Additionally, positional verification was performed using a laser displacement gauge (IL-300; Keyence Corp., Osaka, Japan), with a positional accuracy of 0.05 mm. The laser displacement gauge was used for independent validation of IR Tracking and was not part of the Vero4DRT IR Tracking system. In the experiment, the target position was measured with the

## Accuracy verification of IR Tracking with the Vero4DRT

laser displacement gauge every 10 ms for independent validation, and the laser displacement  
165 signals were sent to a system controller for synchronization of the data recording. The  
Vero4DRT records IR Tracking logs into the system controller every 5 ms. Based on the  
recorded tracking orientation of the gimbaled x-ray head, the tracked position of the target on  
the isocenter plane was calculated as follows:

$$y_t = -960 \tan(\theta_T),$$

170 where  $y_t$  is the tracked position of the target in the CC direction,  $\theta_T$  is the tilt angle of the  
gimbaled x-ray head, and 960 mm is the distance from the rotation center of the gimbals to the  
isocenter. The positional tracking error ( $E_P$ ) was defined as  $E_P = y_t - y_{ml}$ , where  $y_{ml}$  is the  
phantom position in the CC direction, measured with the laser displacement gauge. The 95<sup>th</sup>  
percentile of the  $E_P$  ( $E_P^{95}$ ) was then calculated.

### II. B. 2. Positional verification of IR Tracking for 1D phase-shifted sinusoidal patterns

Figure 3(b) shows a photograph of the experimental system for the positional  
verification of IR Tracking for the 1D phase-shifted sinusoidal patterns ( $A$ : 20 mm,  $T$ : 4 s,  
phase shift [ $\tau$ ]: 0.2-2 s):

$$\begin{aligned} y_p(t) &= 0.5A \sin(\omega t/T), \\ z_s(t) &= 0.5A \sin\{\omega(t - \tau)/T\}, \end{aligned}$$

where  $y_p(t)$  is the phantom position in the CC direction and  $z_s(t)$  is the displacement of the IR  
markers in the AP direction. Positional accuracy was evaluated using the dynamic  
anthropomorphic thorax phantom (CIRS Inc., Norfolk, VA) with a high precision (0.1 mm)  
185 laser displacement gauge.  $E_P^{95}$  was estimated as described in Section II. B. 1.

### II. B. 3. Positional verification of IR Tracking for 3D respiratory patterns

Figure 3(c) shows a photograph of the experimental system for the positional

## Accuracy verification of IR Tracking with the Vero4DRT

verification of IR Tracking with the 3D respiratory patterns acquired from six lung cancer patients. IR markers for measurement using Polaris Spectra (Northern Digital Inc., Waterloo, Ontario, Canada) and fiducial markers for measurement using the gantry-mounted orthogonal kV x-ray imaging subsystem were attached to the surface of a cubic phantom. The Polaris Spectra was used for independent validation of IR Tracking and was not part of the Vero4DRT IR Tracking system. Then, the cubic phantom was placed firmly on the 3D-driven base of a four-axis moving phantom, which moved three-dimensionally, based on the acquired internal target motions. Other IR markers for IR Tracking were also placed on the 1D driven base of the four-axis moving phantom, which moved based on the acquired IR marker motions in the AP direction only. The four-axis moving phantom was able to reproduce patient respiratory motions with high precision (0.1 mm).<sup>23</sup> The positions of the IR markers for measurement ( $P_{mP}[x_{mP}, y_{mP}, z_{mP}]$ ) and fiducial markers for measurement ( $P_{mX}[x_{mX}, y_{mX}, z_{mX}]$ ) were measured with the Polaris Spectra, with a measurement accuracy of 0.3 mm, every 16.7 ms, and by the gantry-mounted orthogonal kV x-ray imaging subsystem every 1 s, respectively. In the present study, these positional data were recorded synchronously, based on the exposers signal of the orthogonal kV x-ray imaging subsystem.

First, the detection accuracy of the gantry-mounted orthogonal kV x-ray imaging subsystem was evaluated in the stationary condition using the treatment couch, with a positional accuracy of 0.01 mm. Second, in total, 742 comparisons between  $P_{mP}$  and  $P_{mX}$  were made to evaluate the detection accuracy of the gantry-mounted orthogonal kV x-ray imaging subsystem in the moving condition using the Polaris Spectra and the four-axis moving phantom.

To investigate the tracking accuracy in each direction, positional verification was performed at gantry angles of 0° and 90°. Based on the recorded tracking orientation of the gimbaled x-ray head, the tracked position of the target was estimated on the perpendicular

## Accuracy verification of IR Tracking with the Vero4DRT

plane to the home gimbal-axis at the measured target position.<sup>10</sup> At a gantry angle of 0°, the

215 tracked position of the target was calculated as follows:

$$x_t = (960 - z_{mX}) \tan(\theta_p),$$

$$y_t = -(960 - z_{mX}) \tan(\theta_T),$$

where  $x_t$  is the tracked position of the target in the lateral (LR) direction,  $\theta_p$  is the pan angle of the gimbaled x-ray head,  $y_t$  is the tracked position of the target in the CC direction, and  $\theta_T$

220 is the tilt angle of the gimbaled x-ray head. At a gantry angle of 0°, the tracked position of the target at the gantry angle of 90° was calculated as follows:

$$y_t = -(960 - x_{mX}) \tan(\theta_T),$$

$$z_t = (960 - x_{mX}) \tan(\theta_p),$$

where  $z_t$  is the tracked position of the target in the AP direction. The  $E_p$  was defined as

225 follows:

$$E_p = \begin{pmatrix} x_t \\ y_t \\ z_t \end{pmatrix} - \begin{pmatrix} x_{mX} \\ y_{mX} \\ z_{mX} \end{pmatrix}.$$

$E_p^{95}$  was estimated as described in Sections II. B. 1. and II. B. 2.

## 230 III. RESULTS AND DISCUSSION

### III. A. Dosimetric and positional verification of IR Tracking for 1D sinusoidal patterns

Figure 4(a) shows dose profiles of a 50×50-mm<sup>2</sup> field under stationary, tracking, and non-tracking states for the sinusoidal patterns with  $(A, T) = (40 \text{ mm}, 2 \text{ s})$ . The blurred effect, due to phantom motion, was reduced substantially by IR Tracking, comparable with previous

235 results.<sup>9</sup> Figure 4(b) shows variations in the tracked and measured positions of the target for the sinusoidal patterns with  $(A, T) = (40 \text{ mm}, 2 \text{ s})$  in the CC direction. Even for the severe motion



## Accuracy verification of IR Tracking with the Vero4DRT

pattern, the gimbaled x-ray head tracked the target in real time with high accuracy.

Table I summarizes  $\mu + 2SD$  of the absolute 4D-modeling error ( $E_{4DM}^{\mu+2SD}$ ),  $E_D^{95}$ , and  $E_P^{95}$  of 1D sinusoidal patterns.  $E_{4DM}^{\mu+2SD}$  was calculated from the  $\mu$  and SD displayed on the screen of the Vero4DRT in the 4D-modeling phase. Under conditions of perfect correlation between the target and IR marker motions,  $E_{4DM}^{\mu+2SD}$  ranged from 1.4 to 1.9 mm.  $E_D^{95}$  ranged from 11.2 to 29.6 mm in the non-tracking state; however, these values were reduced by 0.0 to 1.2 mm in the tracking state. IR Tracking reduced blurring dramatically and produced a dose-profile slope similar to that of the stationary state. Additionally, the measured and tracked positions of the target were consistent with each other.  $E_P^{95}$  ranged from 1.3 to 1.8 mm in the tracking state and from 9.9 to 19.9 mm in the non-tracking state, and  $E_P^{95}$  in the tracking state was similar to  $E_{4DM}^{\mu+2SD}$ . As shown in Table I,  $E_D^{95}$  was much smaller than twice  $E_P^{95}$  because the randomized dose errors were partially cancelled out at the field edge; thus, assessment of  $E_P^{95}$  represents an alternative safety indicator in terms of determining whether the internal margin for IR Tracking is adequate in clinical practice.

### III. B. Positional verification of IR Tracking for 1D phase-shifted sinusoidal patterns

Table II summarizes the absolute correlation coefficient between the target and IR marker motions ( $|R_{IR}^{target}|$ ),  $E_{4DM}^{\mu+2SD}$ , and  $E_P^{95}$  for phase-shifted sinusoidal patterns. As  $|R_{IR}^{target}|$  became small,  $E_{4DM}^{\mu+2SD}$  and  $E_P^{95}$  increased linearly, from 0.4 to 3.0 mm ( $R = -0.98$ ) and from 0.5 to 2.2 mm ( $R = -0.95$ ), respectively. A strong positive correlation was also found between  $E_{4DM}^{\mu+2SD}$  and  $E_P^{95}$  ( $R = 0.99$ ). In the 4D-modeling process, the 4D model was created to minimize residual errors between the predicted and detected target positions. Thus, the relationship between  $E_P^{95}$  and  $E_D^{95}$  will be almost equivalent even in the presence of a phase shift.

## Accuracy verification of IR Tracking with the Vero4DRT

### III. C. Positional verification of IR Tracking for 3D respiratory patterns

The root mean squares (RMSs) of the detection accuracy of the gantry-mounted orthogonal kV x-ray imaging subsystem under the stationary condition were 0.07, 0.04, and 0.03 mm in the LR, CC, and AP directions, respectively. The RMSs of the detection accuracy of the gantry-mounted orthogonal kV x-ray imaging subsystem under the moving condition were 0.14, 0.39, and 0.15 mm in the LR, CC, and AP directions, respectively. These results show that the gantry-mounted orthogonal kV x-ray imaging subsystem of the Vero4DRT had high detection accuracy, even for moving targets.

Figure 5 shows variations in the target position along the CC direction for the respiratory pattern of the first patient who underwent IR Tracking (Patient No. 3).  $E_p^{95}$  was 1.6 mm for this patient.

Table III summarizes  $E_{4DM}^{\mu+2SD}$  and  $E_p^{95}$  for respiratory patterns. A strong negative correlation between  $|R_{IR}^{target}|$  and  $E_{4DM}^{\mu+2SD}/A$  was observed in each direction [(LR, CC, AP) = (-0.88, -0.90, -0.92)]. A strong positive correlation was also found between  $E_{4DM}^{\mu+2SD}$  and  $E_p^{95}$  in each direction [(LR, CC, AP) = (0.99, 0.98, 1.00)]; thus,  $E_p^{95}$  was readily estimated from  $E_{4DM}^{\mu+2SD}$ . Figure 6 shows accumulated probability histograms (a) as a function of the positional tracking errors and (b) as a function of the tracking efficiency, defined as the  $2E_p^{95}/A$ , in each direction at gantry angles of 0° and 90°. The positional tracking errors were larger in the CC direction than in the other directions [Fig. 6(a)]. However, the tracking efficiencies were the highest in the CC direction [Fig. 6(b)]. Lower tracking efficiencies in other directions than in the CC direction were caused by the small  $|R_{IR}^{target}|$  (Table III). Additionally, tracking accuracy was not degraded by gantry rotation, even at an angle of 90°.

Pepin *et al.* suggested that a dry-run treatment session prior to treatment planning is required to determine patient-specific margins covering positional tracking error during the treatment when performing DTT with the Synchrony Respiratory Tracking System.<sup>22</sup> The

## Accuracy verification of IR Tracking with the Vero4DRT

present study revealed that positional tracking errors were near-identical to 4D-modeling errors, derived from miscorrelation between the target and abdominal wall motions, such as the phase shift or irregular respiration. Thus, users of the Vero4DRT should evaluate the accuracy of the 4D model in a dry-run treatment session, and the following should then be discussed, based on the acquired 4D-modeling accuracy: (1) adding margins to compensate for 4D-modeling errors and (2) conducting respiratory coaching to minimize the phase shift.<sup>24</sup>

The correlation between tumor and surrogate motion is known to change from treatment planning to treatment delivery.<sup>3,25,26</sup> The change in correlation may cause additional tracking errors in IR Tracking; thus, additional margins to compensate for these uncertainties are required, and confirmation of whether the 4D-modeling errors for each fraction are within the margin derived from 4D-modeling errors at treatment planning is recommended. Additionally, Malinowski *et al.* reported that an extended treatment time can lead to miscorrelation between the external surrogate and internal tumor motion, due to baseline drift.<sup>27</sup> During irradiation, we can estimate visually the tracking errors in real time from the implanted fiducial markers – or the tumor itself – on the intra-fractional fluoroscopic images. When these positions deviate systematically from those predicted, due to baseline drift or changes in respiration, remodeling of the 4D model during a treatment fraction is required to perform IR Tracking safely.

## IV. CONCLUSIONS

We verified the dosimetric and positional accuracy of IR Tracking and confirmed its feasibility in clinical practice. IR Tracking reduced substantially motion-induced marginal blurring in the dose distribution. Additionally, positional tracking errors correlated strongly with 4D-modeling errors, which resulted from miscorrelations between target and IR marker motions. Thus, the accuracy of the 4D model must be verified before treatment, and margins

## Accuracy verification of IR Tracking with the Vero4DRT

are required to compensate for 4D-modeling errors.

### ACKNOWLEDGMENTS

315           The authors express their appreciation to the entire technical staff at MHI for  
providing detailed information on the gimbaled x-ray head-tracking system and acquiring the  
experimental data. This research was supported by the Japan Society for the Promotion of  
Science (JSPS) through its “Funding Program for World-Leading Innovative R&D on Science  
and Technology (FIRST Program)” and a Grant-in-Aid for Scientific Research from the  
320   Association for Nuclear Technology in Medicine.

## Accuracy verification of IR Tracking with the Vero4DRT

### REFERENCES

1. “Prescribing, recording and reporting photon beam therapy.” ICRU Report 50,  
International Commission on Radiation Units and Measurements, Bethesda, MD (1993).
- 325 2. “Prescribing, recording and reporting photon beam therapy.” ICRU Report 62  
(Supplement to ICRU Report 50), International Commission on Radiation Units and  
Measurements, Bethesda, MD (1999).
3. P. J. Keall, G. S. Mageras, J. M. Balter, R. S. Emery, K. M. Forster, S. B. Jiang, J. M.  
Kapatoes, D. A. Low, M. J. Murphy, B. R. Murray, C. R. Ramsey, M. B. Van Herk, S. S.
- 330 Vedam, J. W. Wong, and E. Yorke, “The management of respiratory motion in radiation  
oncology report of AAPM task group 76,” *Med. Phys.* **33**, 3874–3900 (2006).
4. S. Dieterich, K. Cleary, W. D’Souza, M. Murphy, K. H. Wong, and P. J. Keall, “Locating  
and targeting moving tumors with radiation beams,” *Med. Phys.* **35**, 5684–5694 (2008).
5. Y. Kamino, K. Takayama, M. Kokubo, Y. Narita, E. Hirai, N. Kawada, T. Mizowaki, Y.
- 335 Nagata, T. Nishidai, and M. Hiraoka, “Development of a four-dimensional image-guided  
radiotherapy system with a gimbaled X-ray head,” *Int. J. Radiat. Oncol. Biol. Phys.* **66**,  
271–278 (2006).
6. Y. Kamino, S. Miura, M. Kokubo, I. Yamashita, E. Hirai, M. Hiraoka, and J. Ishikawa,  
“Development of an ultrasmall C-band linear accelerator guide for a four-dimensional
- 340 image-guided radiotherapy system with a gimbaled x-ray head,” *Med. Phys.* **34**,  
1797–1808 (2007).
7. A. Sawada, S. Kaneko, K. Takayama, K. Nagano, Y. Miyabe, M. Nakamura, Y. Narita, K.  
Takahashi, M. Kokubo, T. Mizowaki, and M. Hiraoka, “Daily verification of isocenter  
alignment for a new image guided radiotherapy system, MHI-TM2000,” *Med. Phys.* **36**,
- 345 2586–2587 (2009).
8. M. Nakamura, A. Sawada, Y. Ishihara, K. Takayama, T. Mizowaki, S. Kaneko, M.

## Accuracy verification of IR Tracking with the Vero4DRT

- Yamashita, H. Tanabe, M. Kokubo, and M. Hiraoka, “Dosimetric characterization of a multileaf collimator for a new four-dimensional image-guided radiotherapy system with a gimbaled x-ray head, MHI-TM2000,” *Med. Phys.* **37**, 4684–4691 (2010).
- 350 9. K. Takayama, T. Mizowaki, M. Kokubo, N. Kawada, H. Nakayama, Y. Narita, K. Nagano, Y. Kamino, and M. Hiraoka, “Initial validations for pursuing irradiation using a gimbals tracking system,” *Radiother. Oncol.* **93**, 45–49 (2009).
10. N. Mukumoto, M. Nakamura, A. Sawada, K. Takahashi, Y. Miyabe, K. Takayama, T. Mizowaki, M. Kokubo, and M. Hiraoka, “Positional accuracy of novel  
355 x-ray-image-based dynamic tumor-tracking irradiation using a gimbaled MV x-ray head of a Vero4DRT (MHI-TM2000),” *Med. Phys.* **39**, 6287–6296 (2012).
11. Y. Miyabe, A. Sawada, K. Takayama, S. Kaneko, T. Mizowaki, M. Kokubo, and M. Hiraoka, “Positioning accuracy of a new image-guided radiotherapy system,” *Med. Phys.* **38**, 2535–2541 (2011).
- 360 12. Weiss E, Vorwerk H, Richter S, and C. F. Hess, “Interfractional and intrafractional accuracy during radiotherapy of gynecologic carcinomas: a comprehensive evaluation using the ExacTrac system,” *Int. J. Radiat. Oncol. Biol. Phys.* **56**, 69–79 (2003).
13. T. Depuydt, D. Verellen, O. Haas, T. Gevaert, N. Linthout, M. Duchateau, K. Tournel, T. Reynders, K. Leysen, M. Hoogeman, G. Storme, and M. De Ridder, “Geometric accuracy  
365 of a novel gimbals based radiation therapy tumor tracking system,” *Radiother. Oncol.* **98**, 365–372 (2011).
14. K. Takayama, N. Kawada, K. Nagano, Y. Sato, Y. Matsuo, T. Mizowaki, M. Kokubo, H. Nakayama, Y. Narita, and M. Hiraoka, “Imaging dose on a dual on-board kV x-ray imaging system in MHI-TM2000,” *Int. J. Radiat. Oncol. Biol. Phys.* **72**, S655–S656  
370 (2008).
15. M. J. Murphy, J. Balter, S. Balter, J. A. BenComo, I. J. Das, S. B. Jiang, C. M. Ma, G. H.

## Accuracy verification of IR Tracking with the Vero4DRT

Olivera, R. F. Rodebaugh, K. J. Ruchala, H. Shirato, and F. F. Yin, “The management of imaging dose during image-guided radiotherapy: report of the AAPM Task Group 75,” *Med. Phys.* **34**, 4041–4063 (2007).

- 375 16. M. K. Islam, T. G. Purdie, B. D. Norrlinger, H. Alasti, D. J. Moseley, M. B. Sharpe, J. H. Siewerdsen, and D. A. Jaffray, “Patient dose from kilovoltage cone beam computed tomography imaging in radiation therapy,” *Med. Phys.* **33**, 1573–1582 (2006).
17. C. L. Perkins, T. Fox, E. Elder, D. A. Kooby, C. A. Staley, and J. Landry, “Image-guided radiation therapy (IGRT) in gastrointestinal tumors,” *JOP.* **7**, 372–381 (2006).
- 380 18. A. Schweikard, H. Shiomi, and J. Adler, “Respiration tracking in radiosurgery,” *Med. Phys.* **31**, 2738–2741 (2004).
19. Y. Seppenwoolde, R. I. Berbeco, S. Nishioka, H. Shirato, and B. Heijmen, “Accuracy of tumor motion compensation algorithm from a robotic respiratory tracking system: a simulation study,” *Med. Phys.* **34**, 2774–2784 (2007).
- 385 20. E. Nioutsikou, Y. Seppenwoolde, J. R. Symonds-Tayler, B. Heijmen, P. Evans, and S. Webb, “Dosimetric investigation of lung tumor motion compensation with a robotic respiratory tracking system: an experimental study,” *Med. Phys.* **35**, 1232–1240 (2008).
21. M. Hoogeman, J. B. Prévost, J. Nuytens, J. Pöll, P. Levendag, and B. Heijmen, “Clinical accuracy of the respiratory tumor tracking system of the cyberknife: assessment by analysis of log files,” *Int. J. Radiat. Oncol. Biol. Phys.* **74**, 297–303 (2009).
- 390 22. E. W. Pepin, H. Wu, Y. Zhang, and B. Lord, “Correlation and prediction uncertainties in the cyberknife synchrony respiratory tracking system,” *Med. Phys.* **38**, 4036–4044 (2011).
23. H. Nakayama, T. Mizowaki, Y. Narita, and M. Hiraoka, “Development of a three-dimensionally movable phantom system for dosimetric verifications,” *Med. Phys.* **35**, 1643–1650 (2008).
- 395

## Accuracy verification of IR Tracking with the Vero4DRT

24. M. Nakamura, Y. Narita, Y. Matsuo, M. Narabayashi, M. Nakata, A. Sawada, T. Mizowaki, Y. Nagata, and M. Hiraoka, “Effect of audio coaching on correlation of abdominal displacement with lung tumor motion,” *Int. J. Radiat. Oncol. Biol. Phys.* **75**, 558-563 (2009).
25. K. J. Redmond, D. Y. Song, J. L. Fox, J. Zhou, C. N. Rosenzweig, and E. Ford, “Respiratory motion changes of lung tumors over the course of radiation therapy based on respiration-correlated four-dimensional computed tomography scans,” *Int. J. Radiat. Oncol. Biol. Phys.* **75**, 1605–1612 (2009).
26. S. S. Korreman, T. Juhler-Nøttrup, and A. L. Boyer, “Respiratory gated beam delivery cannot facilitate margin reduction, unless combined with respiratory correlated image guidance,” *Radiother. Oncol.* **98**, 365–372 (2008).
27. K. Malinowski, T. J. McAvoy, R. George, S. Dietrich, and W. D. D’Souza, “Incidence of changes in respiration-induced tumor motion and its relationship with respiratory surrogates during individual treatment fractions,” *Int. J. Radiat. Oncol. Biol. Phys.* **82**, 1665–1673 (2012).



## Accuracy verification of IR Tracking with the Vero4DRT

### FIGURE LEGENDS

**Figure 1.** Schematic diagram of the Vero4DRT.

**Figure 2.** Schematic diagram of infrared (IR) marker-based dynamic tumor-tracking irradiation (IR Tracking). In the 4D-modeling phase, the mean and standard deviation of the absolute 4D-modeling error, as well as the peak-to-peak amplitude of the target motion, are shown on the screen of the Vero4DRT. The right four groups of waves, from top to bottom, show variations in the IR markers' positions in the anteroposterior (AP) direction and the target positions in the lateral (LR), craniocaudal (CC), and AP directions, respectively. In the graphs of the target position, dark-colored waves show the detected target position and light-colored waves show the predicted target position. During beam delivery, the future 3D target position is calculated from the displacements of the IR markers using the 4D model, and then the corresponding tracking orientation is transferred continuously to the gimbaled x-ray head.

**Figure 3.** Photograph of the experimental system for (a) dosimetric and positional verification of infrared (IR) marker-based dynamic tumor-tracking (IR Tracking) of 1D sinusoidal patterns, (b) positional verification of 1D phase-shifted sinusoidal patterns, and (c) positional verification of the 3D respiratory patterns of six patients with lung cancer.

**Figure 4.** (a) Dose profile of a  $50 \times 50 \text{ mm}^2$  field under stationary, tracking, and non-tracking states and (b) variations in the tracked and measured positions of the target for the sinusoidal pattern with a peak-to-peak amplitude of 40 mm and breathing period of 2 s.

435

**Figure 5.** Variations in the target position along the craniocaudal (CC) direction for the

## Accuracy verification of IR Tracking with the Vero4DRT

respiratory pattern of the first patient who underwent IR Tracking (Patient No. 3). Square symbols indicate the detected positions of the target, solid lines with round symbols indicate the tracked positions of the target, and dotted lines show positional tracking errors.

440

**Figure 6.** Accumulated probability histogram (a) as a function of the 95<sup>th</sup> percentile of the positional tracking error ( $E_p^{95}$ ) and (b) as a function of the tracking efficiency, defined as the ratio of twice the 95<sup>th</sup> percentile of the positional tracking error ( $E_p^{95}$ ) to the peak-to-peak amplitude ( $A$ ), in the lateral (LR), craniocaudal (CC), and anteroposterior (AP) directions under gantry angles of 0° (G0deg) and 90° (G90deg).

445

**TABLES****TABLE I.**  $E_{4DM}^{\mu+2SD}$ ,  $E_D^{95}$ , and  $E_P^{95}$  under non-tracking and tracking states for sinusoidal patterns.

Case	$A$ [mm]	$T$ [s]	$E_{4DM}^{\mu+2SD}$ [mm]	Non-tracking		Tracking	
				$E_D^{95}$ [mm]	$E_P^{95}$ [mm]	$E_D^{95}$ [mm]	$E_P^{95}$ [mm]
1	40	2	1.8	29.6	19.9	1.2	1.8
2	40	4	1.9	29.4	19.9	0.2	1.8
3	20	2	1.4	11.2	9.9	0.0	1.3

Abbreviations:  $\mu$  = mean; SD = standard deviation;  $E_{4DM}^{\mu+2SD} = \mu + 2SD$  of the absolute 4D-modeling error;  $E_D^{95}$  = differences in the width of the 95% dose profile between stationary and moving conditions;  $E_P^{95}$  = 95<sup>th</sup> percentile of the positional tracking error;

450  $A$  = peak-to-peak amplitude;  $T$  = breathing period.

**TABLE II.**  $|R_{IR}^{target}|$ ,  $E_{4DM}^{\mu+2SD}$ , and  $E_P^{95}$  of phase-shifted sinusoidal patterns with a peak-to-peak amplitude of 20 mm and breathing period of 4 s.

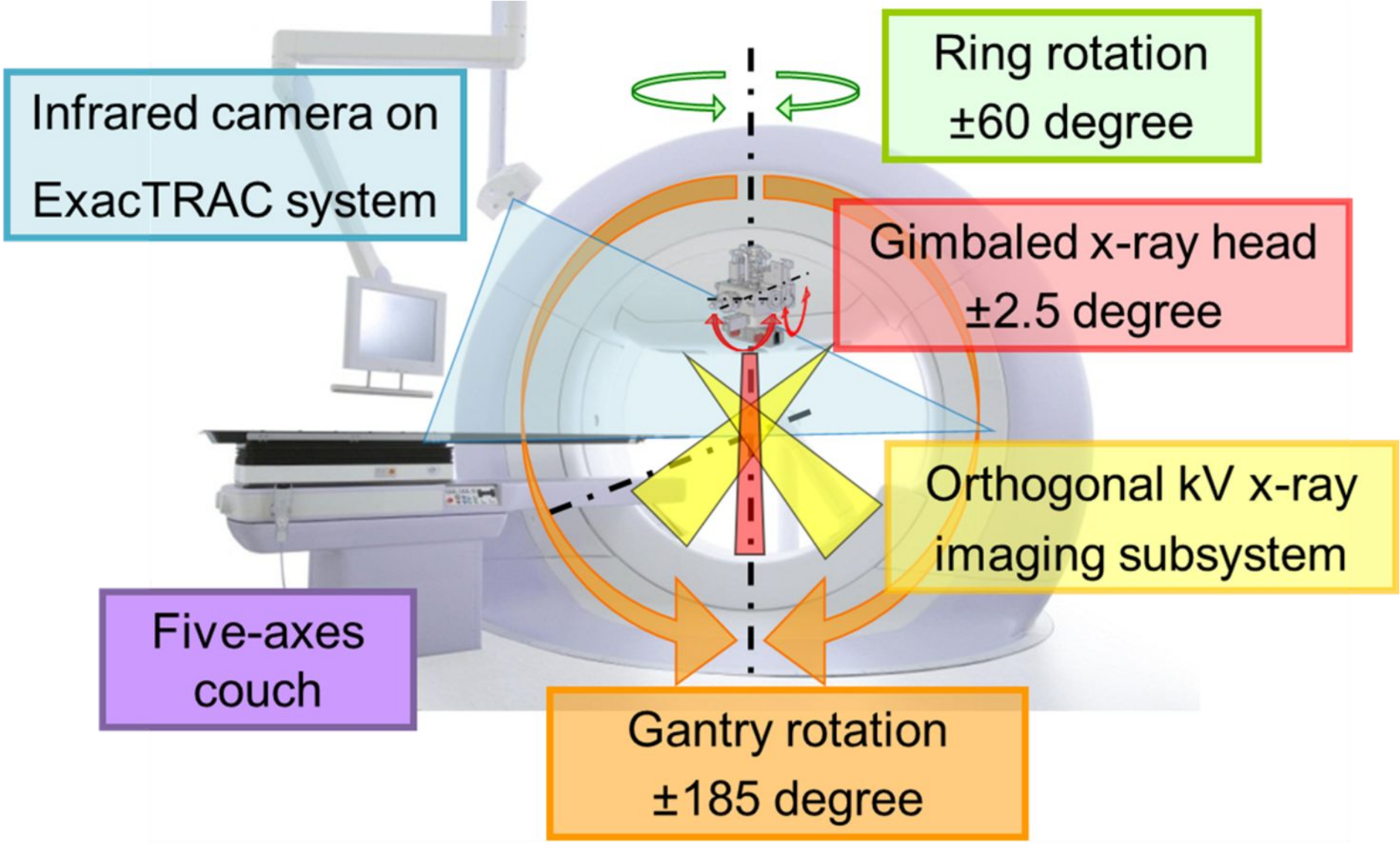
Case	$\tau$ [s]	$ R_{IR}^{target} $	$E_{4DM}^{\mu+2SD}$ [mm]	$E_P^{95}$ [mm]
1	0.0	1.00	0.4	0.6
2	0.2	0.95	0.6	0.7
3	0.4	0.82	1.4	1.4
4	1.0	0.10	3.0	2.2
5	2.0	1.00	0.4	0.5

455 Abbreviations:  $|R_{IR}^{target}|$  = absolute correlation coefficient between target and IR marker motions;  $\mu$  = mean; SD = standard deviation;  $E_{4DM}^{\mu+2SD}$  =  $\mu+2SD$  of the absolute 4D-modeling error;  $E_P^{95}$  = 95<sup>th</sup> percentile of the positional tracking error;  $\tau$  = phase shift.

460 **TABLE III.**  $|R_{IR}^{target}|$ ,  $E_{4DM}^{\mu+2SD}$  and  $E_p^{95}$  of respiratory patterns.

Patient no.	$A$ [mm]			$T$ [s]	$ R_{IR}^{target} $			$E_{4DM}^{\mu+2SD}$ [mm]			$E_p^{95}$ [mm]		
	LR	CC	AP		LR	CC	AP	LR	CC	AP	LR	CC	AP
1	2.4	13.9	7.5	3.6	0.78	0.91	0.01	0.6	3.0	3.2	0.7	2.9	2.6
2	2.0	35.2	5.6	5.5	0.41	0.99	0.93	1.0	3.3	1.4	0.9	3.6	1.2
3	1.7	11.9	1.5	3.4	0.98	0.98	0.26	0.2	1.3	0.5	0.2	1.5	0.6
4	4.2	17.0	3.4	3.5	0.92	0.99	0.93	1.2	2.5	0.4	1.2	2.6	0.5
5	1.7	21.2	3.3	3.4	0.97	0.98	0.92	0.3	2.4	0.5	0.3	2.4	0.6
6	0.7	10.7	2.6	3.1	0.17	0.99	0.60	0.3	1.0	0.7	0.3	1.0	0.8

Abbreviations:  $|R_{IR}^{target}|$  = absolute correlation coefficient between target and IR marker motions;  $\mu$  = mean; SD = standard deviation;  $E_{4DM}^{\mu+2SD}$  =  $\mu+2SD$  of the absolute 4D-modeling error;  $E_p^{95}$  = 95<sup>th</sup> percentiles of the positional tracking error;  $A$  = peak-to-peak amplitude;  $T$  = breathing period; LR = lateral direction; CC = craniocaudal direction; AP = anteroposterior direction.



Infrared camera on  
ExacTRAC system

The diagram illustrates the ExacTRAC system, a robotic platform for radiation therapy. It features a large, light-blue gantry that can rotate around a central vertical axis. A patient is positioned on a five-axis couch that can move in multiple directions. An infrared camera is mounted on a boom above the couch. A gimbaled x-ray head is attached to the gantry, capable of rotating around its own axis. Two orthogonal kV x-ray imaging subsystems are also shown, providing real-time imaging of the patient's position. The gantry's rotation range is ±185 degrees, the ring's rotation is ±60 degrees, and the gimbaled x-ray head's rotation is ±2.5 degrees.

Ring rotation  
 $\pm 60$  degree

Gimbaled x-ray head  
 $\pm 2.5$  degree

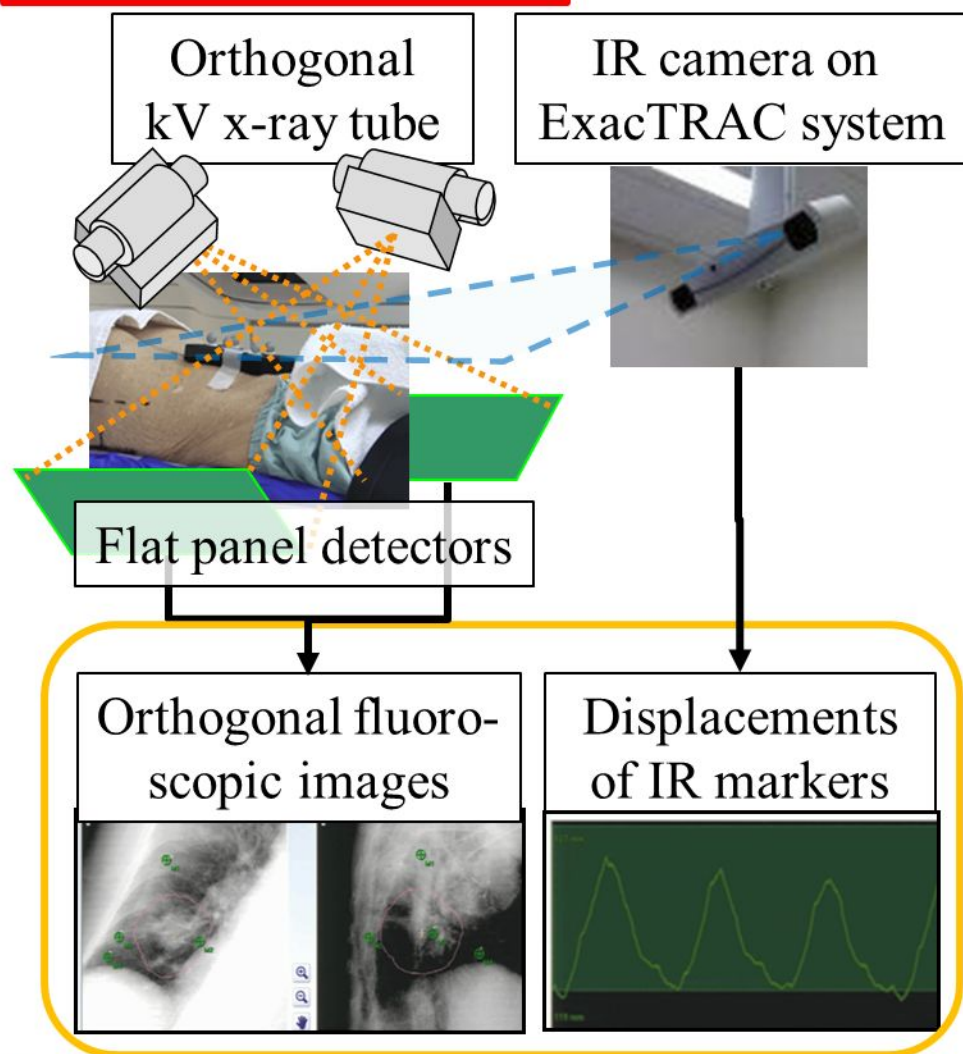
Orthogonal kV x-ray  
imaging subsystem

Five-axes  
couch

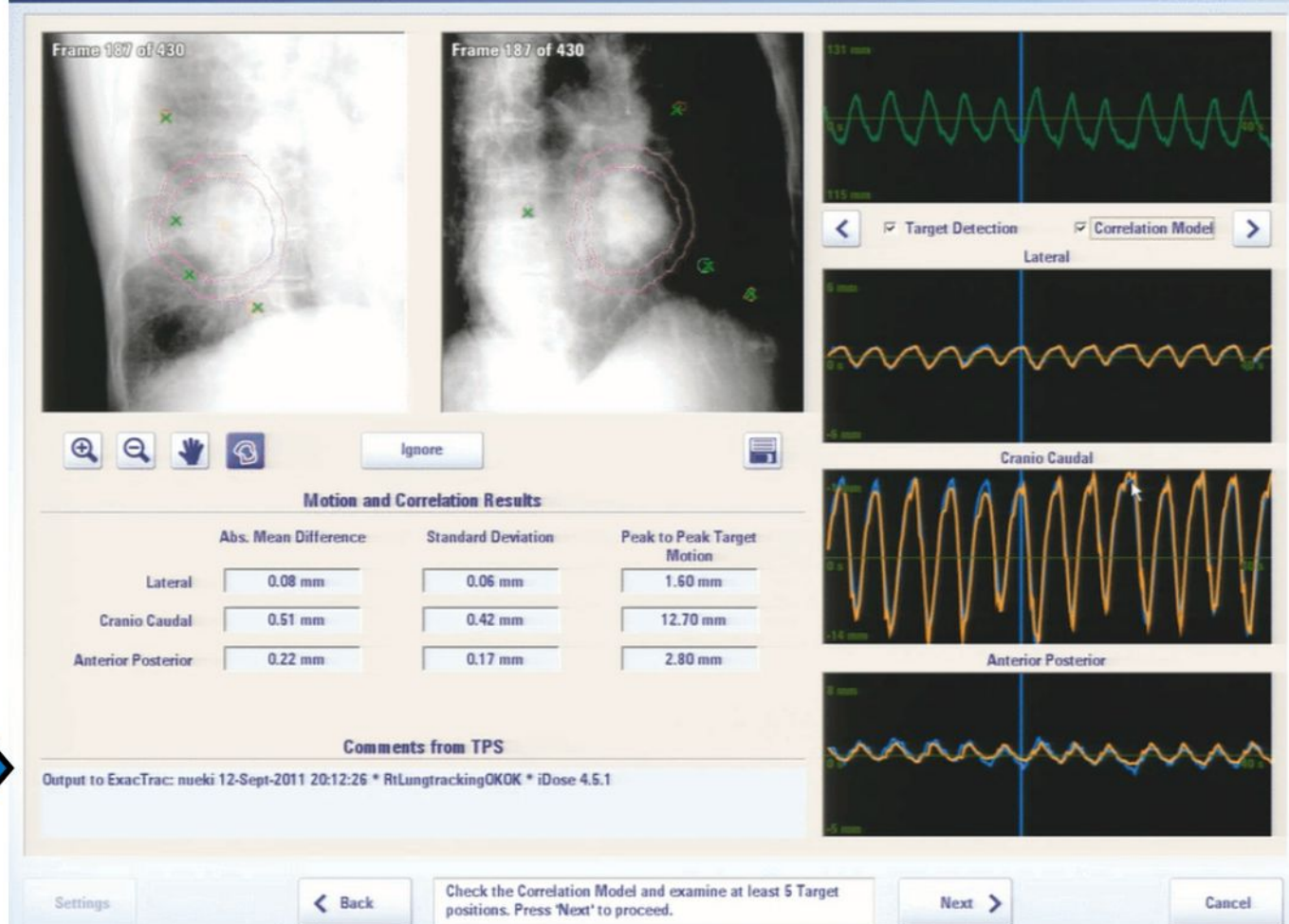
Gantry rotation  
 $\pm 185$  degree



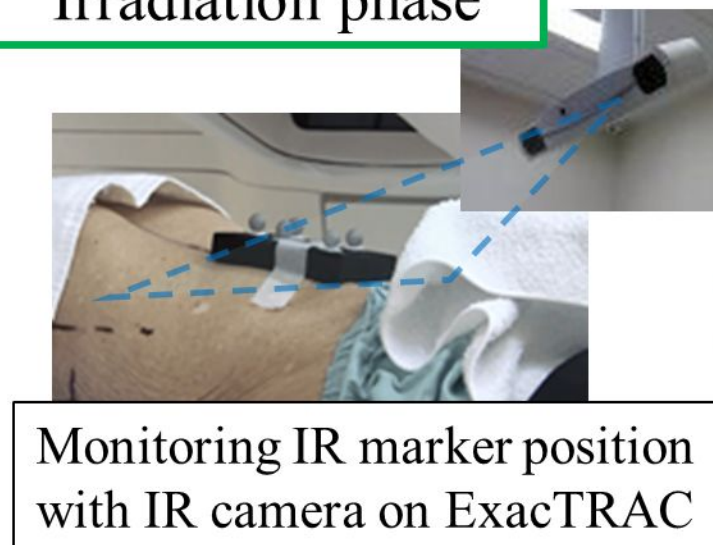
## 4D-modeling phase



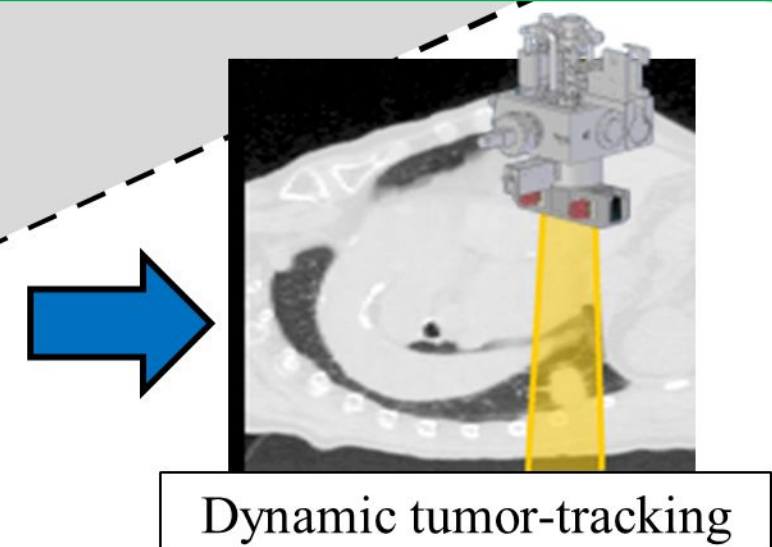
## Screen of the Vero4DRT for the 4D-modeling phase



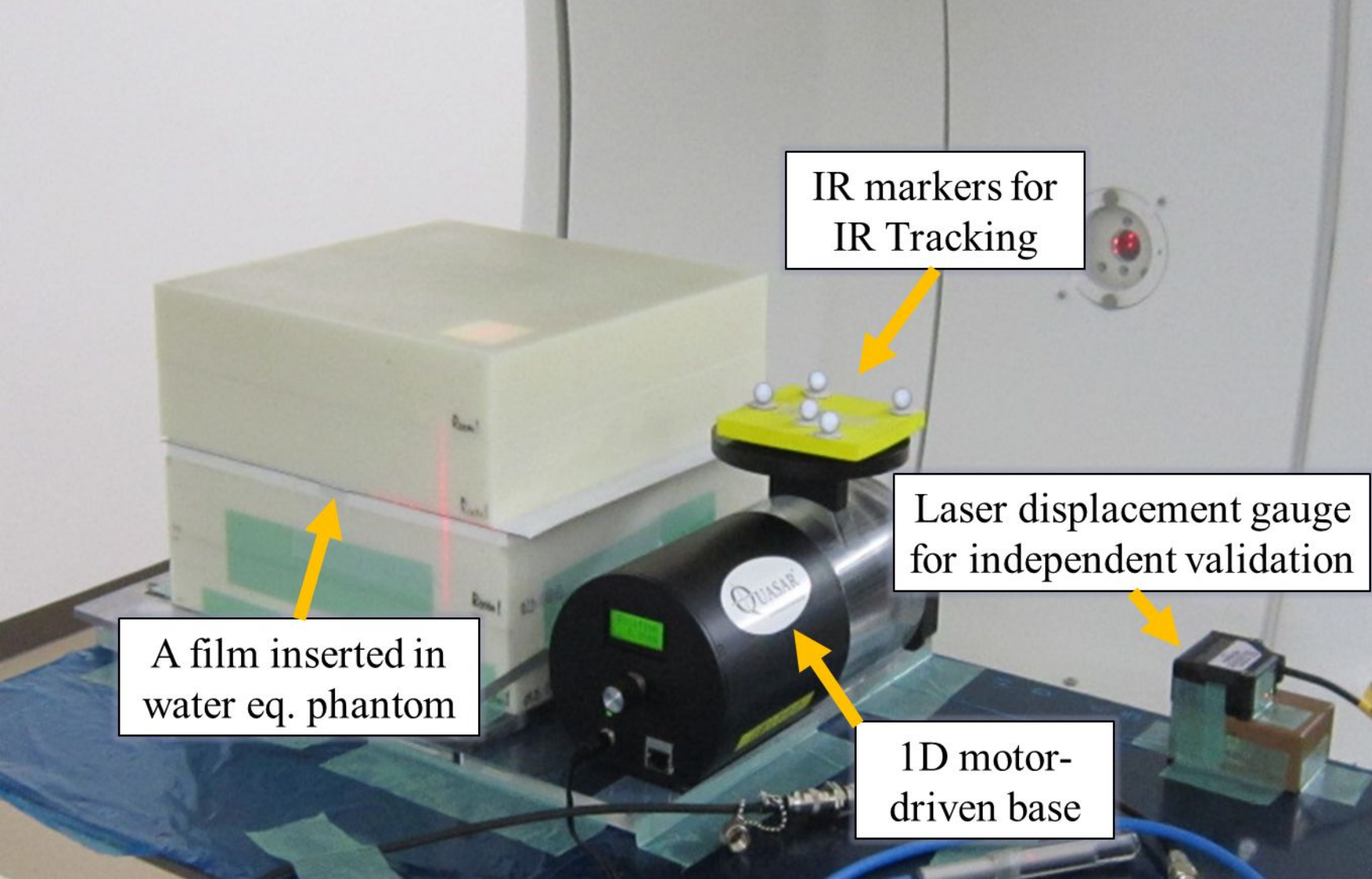
## Irradiation phase



Calculating 3D target position  
by 4D model



Dynamic tumor-tracking



IR markers for  
IR Tracking

Laser displacement gauge  
for independent validation

A film inserted in  
water eq. phantom

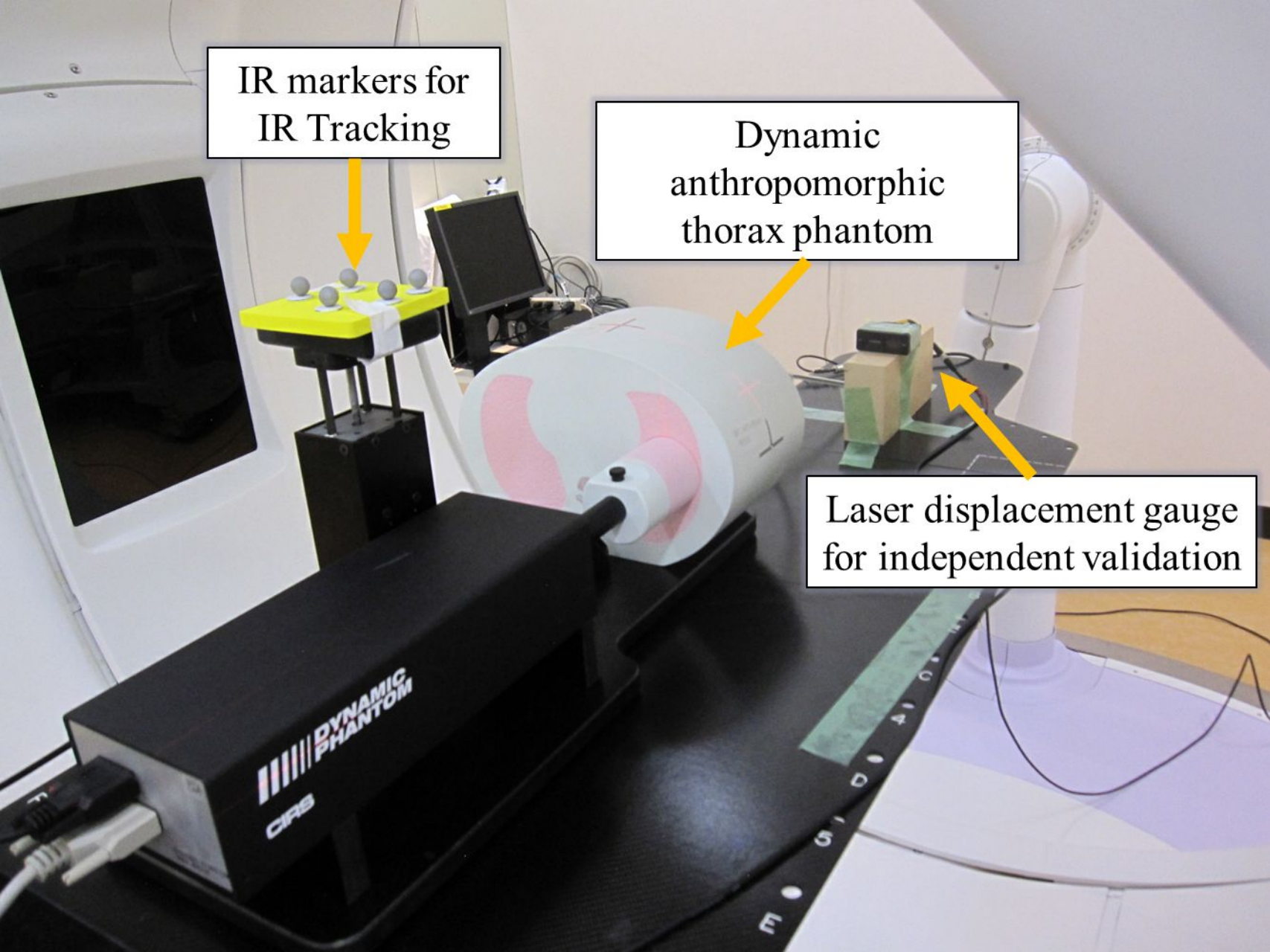
1D motor-  
driven base

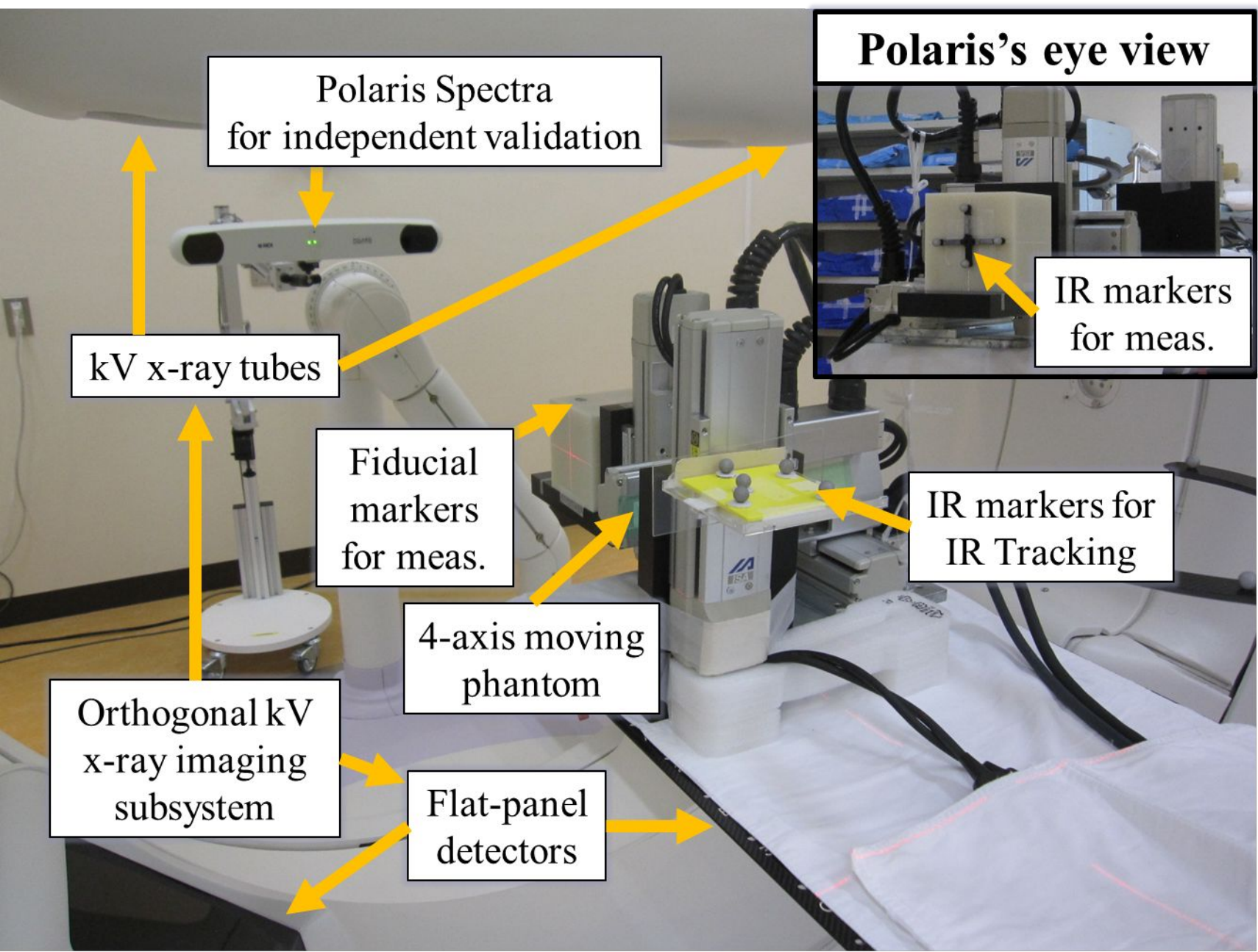


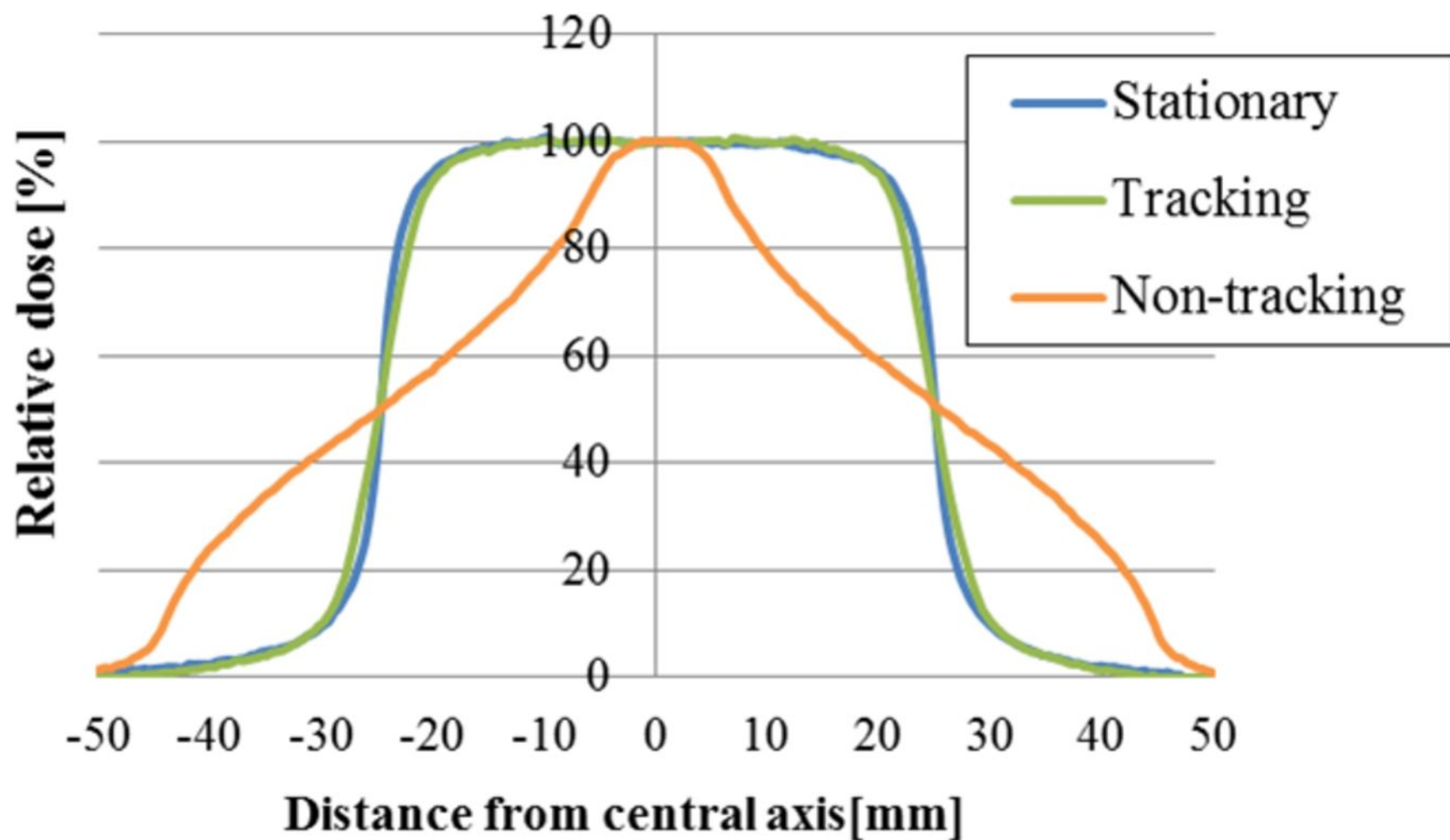
IR markers for  
IR Tracking

Dynamic  
anthropomorphic  
thorax phantom

Laser displacement gauge  
for independent validation









Position along the CC direction

[mm]

